ADVANCED FUNCTIONAL MATERIALS
www.afm-journal.de

Near-Linear Controllable Synthesis of Mesoporosity in Hierarchical UiO-66 by Template-Free Nucleation-Competition

Jia-Xin Li, Gang-Gang Chang, Ge Tian, Chun Pu, Ke-Xin Huang, Shan-Chao Ke, Christoph Janiak, and Xiao-Yu Yang**

Hierarchies design of porosity in metal-organic frameworks (MOFs) has gained significant interest in recent years, and customization of mesoporous sizes in MOFs is still quite challenging. Herein, a template-free method by nucleation-competition has been developed to realize a near-linear control of the mesopore sizes (3–13 nm) in the hierarchical MOF UiO-66(Hf). High selectivity of enzyme adsorption, high activity of bulky-molecular catalysis, high stability of mesostructure, and extension to other MOFs further prove the success in the potential customization synthesis and applications.

1. Introduction

Hierarchically porous metal-organic frameworks (HP-MOFs) have become a rapidly evolving field of current interest, and their hierarchy on porosity is crucial for a high-performance design in all kinds of applications.[1–7] Currently, a large series of synthesis methods have been developed, for example, ligand-extension,[8–11] template-assistant,[12–17] and defect-formation strategy.[18–23] One great challenge is customization synthesis of the mesopore size (2–50 nm), which is critical to selective catalysis or adsorption.[24–29] Surfactant and colloidal templating by careful control of phase separation, can be utilized to synthesize the hierarchical pore structure, however meso-structured MOFs are not very stable and usually lead to interpenetration or structural collapse during the removal of the template because of the strong interaction between surfactant micelles and the framework.[30,31] Isoreticular ligand-elongated strategy is a very efficient way to achieve predictable, uniform, and defined mesoporosity, although its limitation is the complicated synthesis process of elongated ligands.[32] A template-free technique would therefore be preferred. Defect-construction by excessive modulator agents,[20] thermolysis,[19] ozonolysis,[21] or etching[22,26,27] are typical template-free approaches. The interparticle nanofusion also yields aggregation-induced mesoporosity for formation of hierarchical MOF materials.[33] However, these template-free methods usually give rise to a wide distribution of meso/macro pore sizes. It is therefore of scientific interesting and technological importance to develop a facile and directed template-free method to construct stable HP-MOFs with precisely tailored mesopore size.

Water is an efficient modulator to significantly decrease the crystal size of MOFs and correspondingly increase the aggregation-induced packing porosity. Water accelerates crystal nucleation by fast hydrolysis of the metal salts and dicarboxylic acid ligands.[34–36] On the other hand, monocarboxylic acids as modulators are often used to grow large single crystals.[37] The monocarboxylate terminal ligands coordinate to the metal atoms, forming soluble metal-carboxylate clusters and thus slow down the formation of MOF nucleation by competition with the bridging dicarboxylate ligands.[38] The two modulators, water, and monocarboxylate, operate in different directions concerning the nucleation rate which is critical to control the MOF crystal size. Water favors fast nucleation and monocarboxylic acids show the opposite effect. It should, thus, be possible to control the nucleation rate by adjusting the ratio of oppositely-acting modulators. Water and monocarboxylic acids alone are incapable of precise control of mesoporosity of a hierarchical MOF.[33,39]

Herein, the MOF UiO-66(Hf) ($Hf_6O_4(OH)_4(BDC)_6$, BDC = 1,4-benzenedicarboxylate), has been chosen for a proof of concept to demonstrate near-linear control and template-free synthesis of mesoporosity of hierarchical MOFs. The mesopore size can be near-linearly tuned in the range of 3 to 13 nm by adjusting the molar ratio of monocarboxylate acid/water. Extension to other UiO-66 series MOFs and high selectivity of

J.-X. Li, Prof. G.-G. Chang, Prof. G. Tian, C. Pu, K.-X. Huang, S.-C. Ke, Prof. X.-Y. Yang
State Key Laboratory of Advanced Technology for Materials Synthesis and Processing & School of Chemistry
Chemical Engineering and Life Science & School of Materials Science and Engineering & International School of Materials Science and Engineering
Wuhan University of Technology
122, Luoshi Road, Wuhan, Hubei 430070, China
E-mail: changgang2016@whut.edu.cn; xyyang@whut.edu.cn, xyyang@seas.harvard.edu
Prof. C. Janiak
Institut für Anorganische Chemie und Strukturchemie
Heinrich-Heine-Universität Düsseldorf
40204, Düsseldorf Germany
Dr. X.-Y. Yang
School of Engineering and Applied Sciences
Harvard University
Cambridge, MA 02138, USA
The ORCID identification number(s) for the author(s) of this article can be found under https://doi.org/10.1002/adfm.202102868.

DOI: 10.1002/adfm.202102868

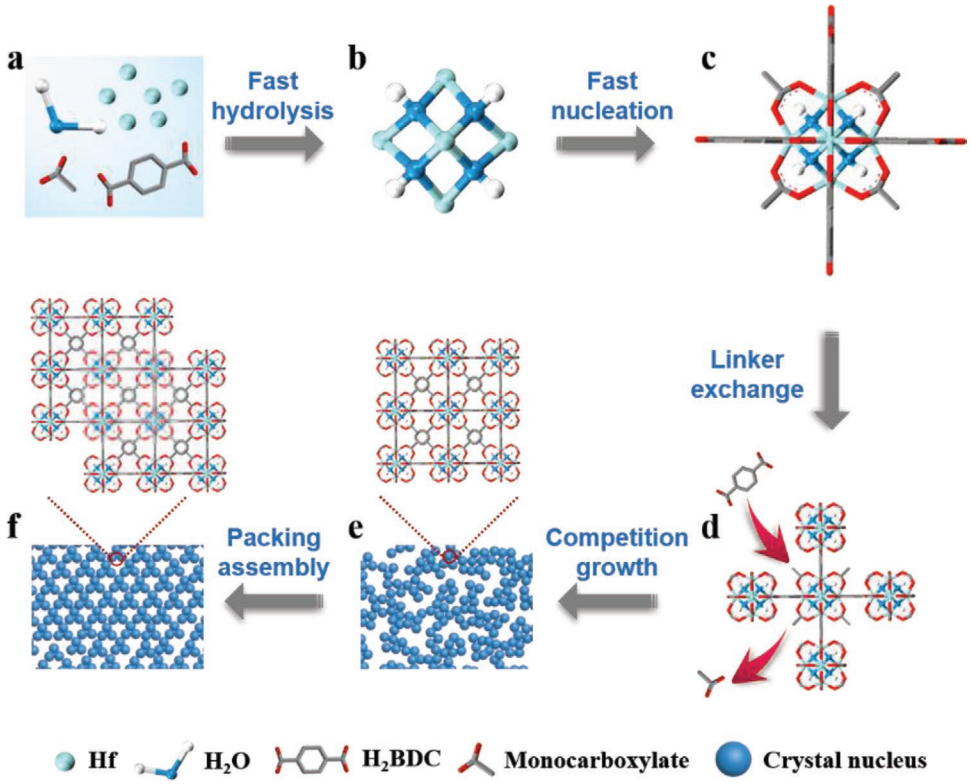

Scheme 1. Schematic illustration of the synthesis of HP-MOFs. a) The solvothermal reaction of $HfCl_4$ and H_2BDC in DMF with water and monocarboxylate as modulators; b) an inner $Hf_6O_4(OH)_4$ core with the triangular faces of the Hf_6-octahedron capped by O and -OH groups; c) a $Hf_6O_4(OH)_4(CO_2)_{12}$ cluster, in which the polyhedron edges are bridged by carboxylates ($-CO_2$) originating from the dicarboxylic acids or monocarboxylic acids; d) linker exchanging procedure, where carboxylate ligand replaces monocarboxylic acid to link the block units as bridge; e) rapidly generated UiO-66 nanoparticles and (inset) the enlarged framework of a single UiO-66 nanoparticle; f) hierarchical MOF with secondary pack mesoporosity by nanoparticles assemble, and (inset) the enlarged nanofusion among UiO-66 nanoparticles.

enzyme adsorption and bulky-molecular catalysis proved the success in the precise synthesis.

2. Results and Discussion

As shown in **Scheme 1** after mixing water, hafnium salt ($HfCl_4$ as an example), monocarboxylic acids (acetic acid as an example), 1,4-dicarboxybenzene, and the solvent DMF (N,N-dimethylformamide), first water would speed up the hydrolysis of hafnium (Hf) salt to generate a large number of $[Hf_6O_4(OH)_4]$ nucleus. And then, monocarboxylic acids and 1,4-benzenedicarboxylate coordinate to hafnium ion of the nucleus, and form a block unit with high ratio of mono/di carboxylate due to the high ratio of the initial sources (mono/di molar ratio is 35). This high ratio of mono/di carboxylate would slow down the uncontrolled aggregation of nucleus and avoid the fast precipitate, because the monocarboxylate stops the linkage of the cluster. By an exchange between monocarboxylic acids and carboxylate ligands at the coordination sites of the Hf, the dicarboxylate acts as bridge to link the block units.[40–42] Finally, the crystal grows and the packing assembly mesopore form. The crystal size therefore depends on the two critical factors of water and monocarboxylate, when the ratio of mono/di carboxylate is fixed. With the increasing ratio of water/monocarboxylate, crystal size decreases, and thus mesopore decreases. Predictably, this direct correlation of inverse relation would occur in certain range. Note that this formation could be done within 5 min in an open system (the detailed formation mechanism in Figure S1, Supporting Information).

The ratios of water/acetic acid (H_2O/CH_3COOH) with 1, 1.5, 2, 3, 4, 5, 6, 7, 8, 9, and 18 have been carried out to demonstrate the proof of concept of design and synthesis of hierarchically porous UiO-66(Hf) (designed as HPU-X, X = ratio of water/monocarboxylate such as 1, 1.5, 2, 3, 4, 5, 6, 7, 8, 9 and 18). Interestingly, the crystal size gradually decreases with the increase of ratio of H_2O/CH_3COOH (Figures S2 and S3, Supporting Information). Notably, the TEM study of the mesostructured particle aggregates not only further confirmed that each nanocrystal had a highly crystalline structure (**Figure 1**b and Figure S4, Supporting Information), where highly crystalline domains can be found with lattice spacings of 0.231 nm representing the (221) crystal plane of UiO-66 MOFs, but also showed that the mesopores were constructed from MOFs nanocrystals which were bonded together by the interconnecting amorphous-crystalline-amorphous region (Figure 1c,d). This is a unique structure, which results in greatly improved stability of the hierarchically porous structure and is also a critical factor in avoiding collapse of the mesopore walls in the final product. Notably, HPU-8 also shows a common structure feature with

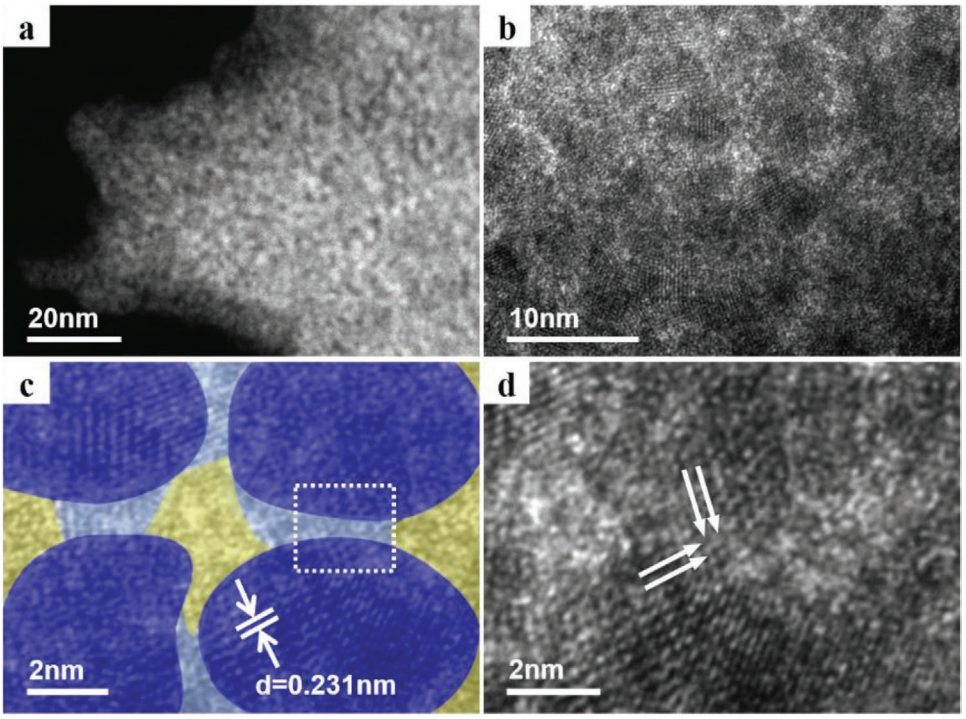

Figure 1. a) STEM image and b) HRTEM images of HPU-6; c) HRTEM image of nanocrystalline domains of HPU-6, and three different regions in three colors that the dark blue area indicates nanoparticles, the pale blue indicates amorphous region, the yellow area indicates packing mesopore; d) enlarged the dotted line part in (c), lattice fusion direction indicated by direction of white arrows in crystal fusion region between two nanoparticles.

clear lattice spacing of 0.260 nm representing the (220) crystal plane of UiO-66 MOFs (Figure S5, Supporting Information).

The precise control of mesostructures can be directly proven by N_2 adsorption-desorption isothermals and the average mesopore distribution are 16.6, 13.1, 12.9, 8.0, 7.9, 7.0, 6.4, 5.1, 5.2 and 3.7 nm, which were in very good agreement with the TEM data (Figure S2 and Table S1, Supporting Information). It has to be pointed out that HPU-4 (8.0 nm), HPU-3 (12.9 nm), HPU-2 (13.1 nm), and HPU-1.5 (16.6 nm) show the wide distribution of pore sizes, although these samples show typical adsorption curve of type IV. Meanwhile, HPU-1 does not show mesoporous structure. For the view of customization synthesis, the near-linear relationship between the mesopore sizes and ratio of water/acetic acid might be in range of 3.7–7.9 nm (red dot-line in **Figure 2**a). The XRD profile of all samples (Figure 2c and Figure S7, Supporting Information) revealed the typical UiO-66 structure, and the diffraction peaks at 7.38° and 8.54° became obviously broadened with the increase of ratio of H_2O/CH_3COOH, attributed to the nanosize reduction of HPU samples. Very little changes for the treated sample under acid and base condition (pH = ≈1–11 for 12 h, respectively) indicated that hierarchical UiO-66(Hf) had excellent chemical stability, critical to acid/base catalysis, directly attributed to the unique bonding structure of MOFs nanocrystals (Figure 2d).

The advantageous feature of mesoporosity includes bulky molecular adsorption and catalysis (Figure S8, Supporting Information, and the corresponding detailed discussion and mechanism of the selective catalysis and adsorption). The bulk molecule tetrakis (4-carboxyphenyl)-porphyrin (TCPP) (≈1.5 nm)[43] could be completely adsorbed by HPU-3 due to its larger pore size (≈13 nm), while the uptake amount of microporous UiO-66(Hf) (0.6 nm) was very low (**Figure 3**a and Figure S9, Supporting Information). The phosphotungstic acid (PTA, ≈1.2 nm) which has been widely utilized as acid catalyst was attempted to be encapsulated into HPU-3 to verify the advantage of HPU in the incorporation of large active sites. The success in the encapsulation of the PTA (Figure S10, Supporting Information), directly results in high activity of the catalytic methanolysis of styrene oxide. For example, after reacting for 40 min, PTA@HPU-3 showed a 92% of the conversion of styrene oxide, although this sample shows the relatively wide pore distribution. The PTA@UiO-66(Hf) only exhibited around 8% conversion (Figure 3b). More importantly, the PTA@HPU-3 showed very high catalytic and structural stability, for example, 95% of initial activity after five consecutive runs (Figures S11–S13 and Table S2, Supporting Information). The very precise tuning of the mesopore size opens a door to high selectivity of molecules' adsorption. The uptake of lysozyme (LSZ, 4.5 nm × 3.0 nm × 3.0 nm)[44] and horseradish peroxidase (HRP, 4.0 nm × 4.4 nm × 6.8 nm)[45] were tested on the resultant HPU-5, HPU-9, and HPU-18 with different pore size (7.9, 5.2, and 3.7 nm). High selectivity involving HPU-9 to LSZ and HPU-5 to HRP suggested the highly uniform pore distribution in HPU samples (Figure 3c,d).

Obviously, the pore size and grain size are dependent on the addition of acid/H_2O, and could be size controlled by using ratio of acid/H_2O. **Figure 4**a shows the relationship of the pore sizes (D = diameter of pore, nm) and molar ratio of acid/H_2O (m = mole number of acetic acid/mole number of water), which is near-linear relation according to the equation: $D = 95.87\ m + 1.84$,

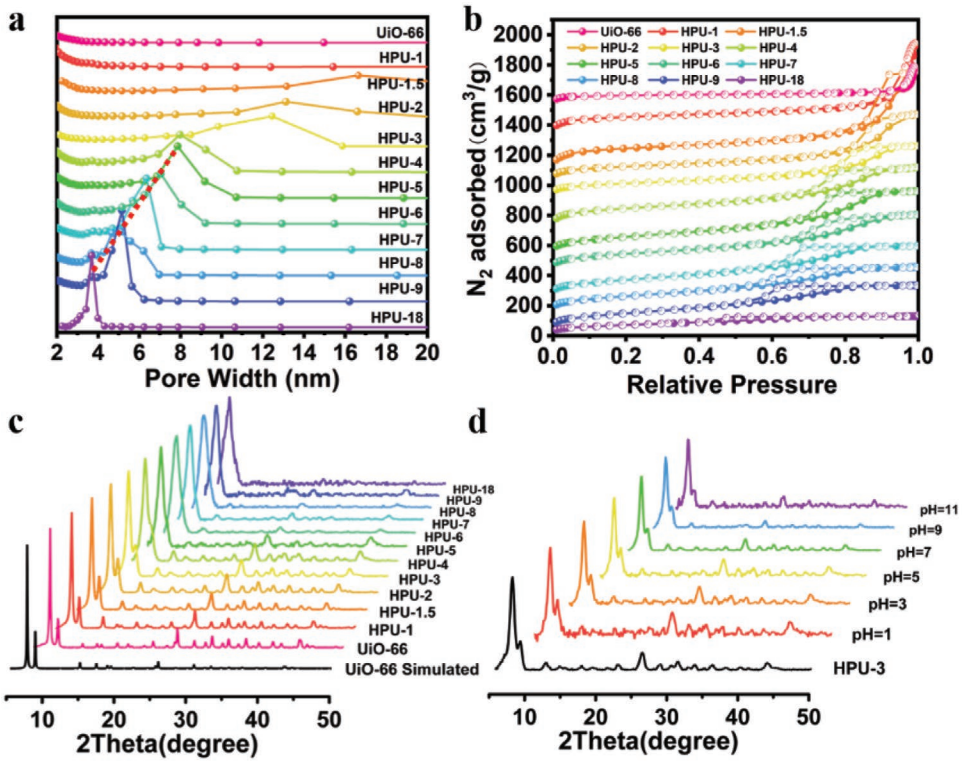

Figure 2. a) Pore size distribution curves, b) nitrogen sorption isotherms and c) XRD patterns of UiO-66 and HPU-X (X = 1, 1.5, 2, 3, 4, 5, 6, 7, 8, 9, and 18); The Barrett–Joyner–Halenda (BJH) model are used to fit the N_2 adsorption isotherm and calculate the pore width. The adsorption isotherms for UiO-66 shifted by 1400 $cm^3\ g^{-1}$. The isotherms from HPU-1 to HPU-8 are shifted by 1300, 1000, 1000, 880, 650, 500, 410, 210 and 140 $cm^3\ g^{-1}$, respectively. d) XRD patterns of HPU-3 treated with various solution (pH = 1–11) for 12 h. The intensities of the XRD patterns are normalized by the (111) diffraction peak intensity ($2\theta = 7.36°$).

where m is in range between 0.0175 and 0.0629. The pore sizes of HPU-4, HPU-3, HPU-2, HPU-1.5, and HPU-1 above-mentioned are not in the range of near-linear control, considering the wide distribution of pore sizes, especially HPU-1 without mesoporous structure (Figure S3, Supporting Information), although most of the pore sizes are in error range and show typical mesostructure. 5 in HPU-5 is limiting ratio of water/acid (m = 0.0629). With the increasing amount of H_2O, crystal size decreases, and thus mesopore occurs and decreases. 18 is considered as another limiting ratio of water/acid (m = 0.0175) because the pore size of HPU-18 is very close to 2 nm and the HPU-20 shows no mesopore and crystalline structure (Figure S15, Supporting Information). A clear conclusion is that with the increasing of the water amount, both crystalline degree mesopores of the samples decrease. To confirm these fitting near-linear relation, 5.5 and 9.5 mL H_2O (and fixed 1 mL of acetic acid) were selected (Figure S14 and Table S1, Supporting Information), which the m values are 0.0572 and 0.0331 and simulative pore sizes are 7.3 and 5.0 calculated by above linear relationship equation, respectively. Very strikingly, the experimental pore sizes (6.9 and 4.9 nm) are well consistent with these two simulative values (Figure 4a), whatever linear and/or second linear relationships. It has to be pointed out that the m value should be in a certain range because the mesoporosity would disappear using a relatively small amount of H_2O (≤1 mL) and/or a relatively large amount of H_2O (≥20 mL) (Figures S15 and S16, Supporting Information). This indicates that the pore size of hierarchical MOFs could be simply designed and controlled by the adjustable ratio of acid/H_2O in a certain range and fixed acid amount.

It is worthy to note that the synthesis of mesopore size-controlled hierarchical MOFs is not only limited to using of acetic acid. Butyric acid and octanoic acid were further chosen to confirm the near-linear relationship. The two types of acids can be used to design and control the pore sizes by near-linear relationship (Figure 4b, Figure S17 and Table S3, Supporting Information). To further understand the effect of different acidic types, various acids, including formic acid (HCOOH), acetic acid (CH_3COOH), propionic acid (CH_3CH_2COOH), butyric acid ($CH_3(CH_2)_2COOH$), caproic acid ($CH_3(CH_2)_4COOH$), octanoic acid ($CH_3(CH_2)_6COOH$), decanoic acid ($CH_3(CH_2)_8COOH$), dodecanoic acid ($CH_3(CH_2)_{10}COOH$), are mixed with a fixing amount of the water (3 mL) (Figures S18–S23 and Table S4, Supporting Information). Very interestingly, the near-linear relationship between the molar ratio and pore size still occurs (Figure 4c). These all near-line relationships shared a core rule that would be in a certain range on basis of a fixing amount of water or acid. More successes in various MOFs such as UiO-66-NH_2(Hf), UiO-66-$(OH)_2$(Hf), UiO-66(Zr), and NUS-6(Hf) were also proved with pores size-control of their mesoporosities and demonstrated a predictable superiority for the bulky molecule catalytic activity (Figures S24–S26, Supporting Information, the corresponding detailed discussion and mechanism of the selective catalysis). It is believed that the strategy developed here

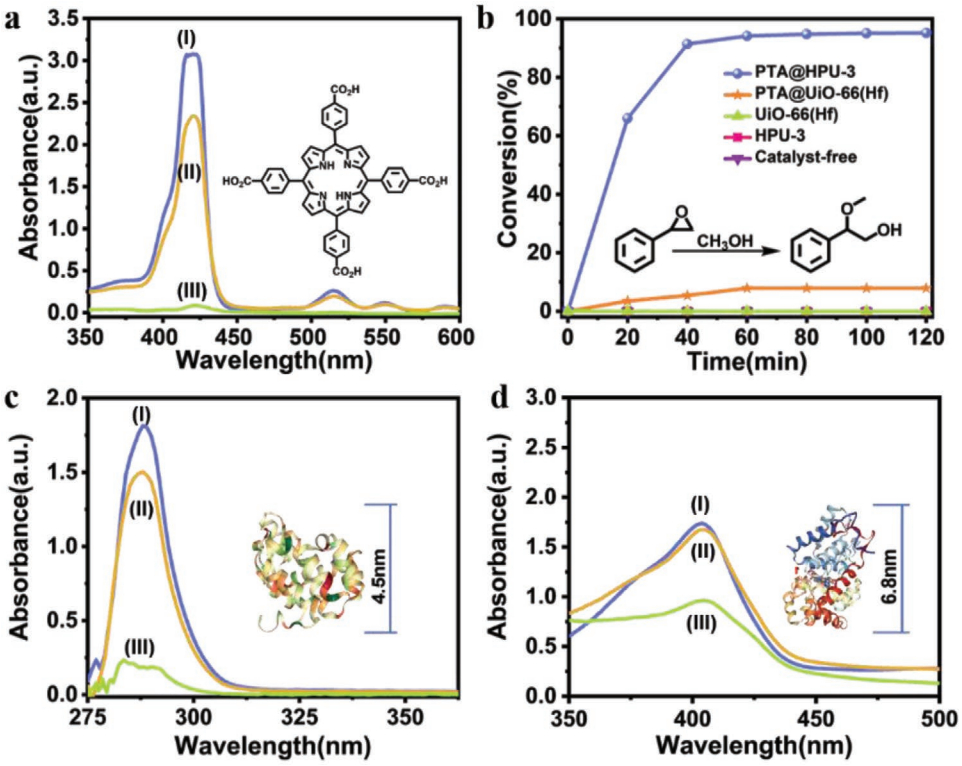

Figure 3. a) UV–vis spectra of (I) the prepared TCPP solution at a concentration of 0.1 mg mL^{-1} and the supernatants after the separation of (II) UiO-66(Hf) (1.5 nm) and (III) HPU-3 (12.9 nm), which the adsorption percentage is 46% and 97%, respectively, and (Inset) the structural formula of TCPP; b) Time conversion of the ring opening of styrene oxide with methanol for varied catalysts, including PTA@HPU-3 showing a 92% of the conversion of styrene oxide in 40 min, and PTA@UiO-66(Hf) only exhibiting ≈8% conversion. (Inset) The equation of catalytic methanolysis of styrene oxide; c) UV–vis spectra of (I) the prepared lysozyme (4.5 nm × 3.0 nm × 3.0 nm) solution at a concentration of 5 mg mL^{-1} and the supernatants after the separation of (II) HPU-18 (3.7 nm) and (III) HPU-9 (5.2 nm), which the adsorption percentage is 35% and 71%, respectively. (Inset) The structure of the lysozyme; d) UV–vis spectra of (I) the prepared horseradish peroxidase (4.0 nm × 4.4 nm × 6.8 nm) solution at a concentration of 1 mg mL^{-1} and the supernatants after the separation of (II) HPU-9 (5.2 nm) and (III) HPU-5 (7.9 nm), which the adsorption percentage is 2% and 50%, respectively. (Inset) The structure of the horseradish peroxidase.

provides a unique, effective, and potentially general approach for the synthesis of hierarchical MOFs with controllable pore size.

Supporting Information

Supporting Information is available from the Wiley Online Library or from the author.

Acknowledgements

This work was supported by a joint National Natural Science Foundation of China-Deutsche Forschungsgemeinschaft (NSFC-DFG) project (NSFC grant 51861135313, DFG JA466/39-1), National Natural Science Foundation of China (21706199), Rapid Response Bilateral Collaborative Funding of the Sino-German Center for Research Promotion (C-0046), International Science & Technology Cooperation Program of China (2015DFE52870).

Conflict of Interest

The authors declare no conflict of interest.

Data Availability Statement

Data available on request from the authors.

Keywords

directed synthesis, heterogeneous catalysis, hierarchical nanostructure, metal-organic frameworks, selective adsorption

Received: April 3, 2021
Published online: May 19, 2021

[1] L. Li, S. Xiang, S. Cao, J. Zhang, G. Ouyang, L. Chen, C.-Y. Su, *Nat. Commun.* **2013**, *4*, 1774.
[2] S. M. Wu, X.-Y. Yang, C. Janiak, *Angew. Chem., Int. Ed.* **2019**, *58*, 12340.
[3] A. E. Baumann, D. A. Burns, B. Liu, V. S. Thoi, *Commun. Chem.* **2019**, *2*, 86.
[4] J. Ying, A. Herbst, Y. X. Xiao, H. Wei, G. Tian, Z. F. Li, X.-Y. Yang, B.-L. Su, C. Janiak, *Inorg. Chem.* **2018**, *57*, 899.
[5] W. Xia, A. Mahmood, R. Zou, Q. Xu, *Energy Environ. Sci.* **2015**, *8*, 1837.

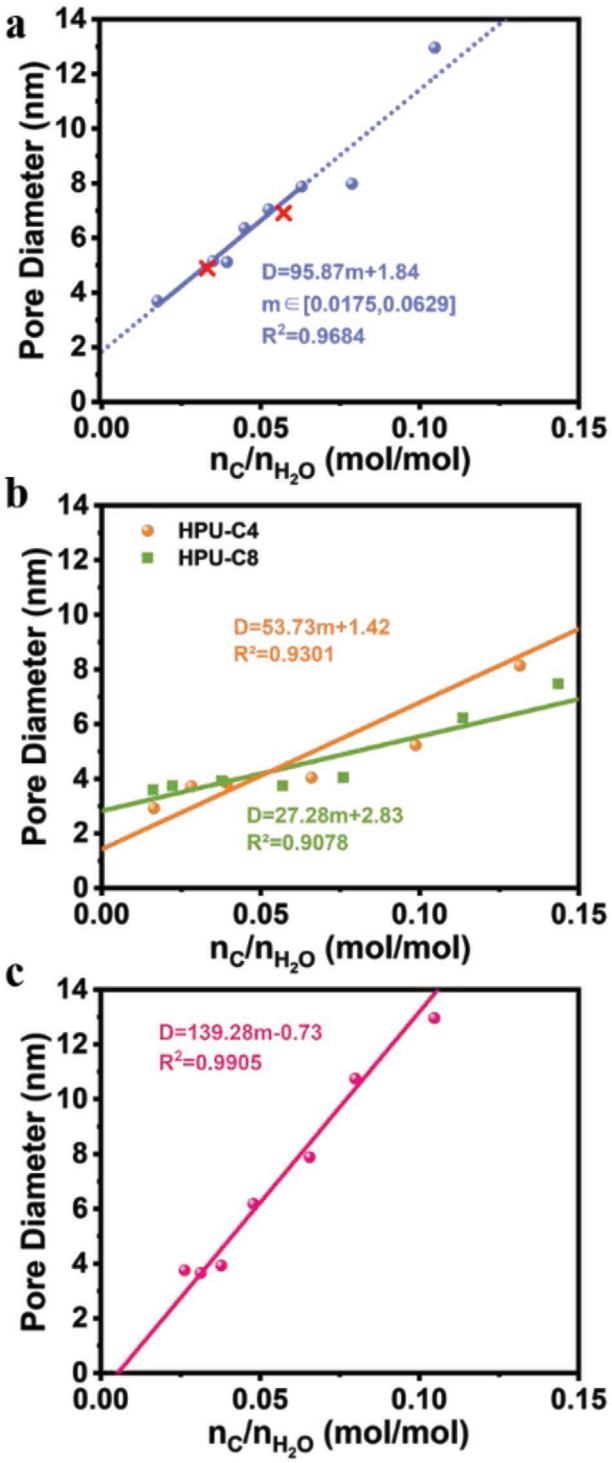

Figure 4. The linear relationship between the pore sizes (diameter) and molar ratio of a) acetic acid/H_2O, b) butyric acid/H_2O, octanoic acid/H_2O, and c) different monocarboxylic acid/H_2O. Equations of inset, (inset of (a)) linear relationship (solid part) and possible near-linear relationship (dot part), (inset of (b)) linear relationship based on HPU-C4 series samples (orange line from round dots) and HPU-C8 series samples (green line from square dots), (inset of (c)) linear relationship based on HPU-Cn series samples. The R^2 is coefficient of determination and all are over 0.9, indicating the regression line has a good fitting degree to the observed values.

[6] C. Pu, J. Zhang, G. G. Chang, Y. Y. Xiao, X. C. Ma, J. Wu, T. T. Luo, K. X. Huang, S. C. Ke, J. X. Li, X.-Y. Yang, *Carbon* **2020**, *159*, 451.
[7] J. Wu, G. G. Chang, Y. Q. Peng, X. C. Ma, S. C. Ke, S. M. Wu, Y. X. Xiao, G. Tian, T. Xia, X.-Y. Yang, *Chem. Commun.* **2020**, *56*, 6297.
[8] O. M. Yaghi, M. O'Keeffe, N. W. Ockwig, H. K. Chae, M. Eddaoudi, J. Kim, *Nature* **2003**, *423*, 705.
[9] O. K. Farha, J. T. Hupp, *Acc. Chem. Res.* **2010**, *43*, 1166.
[10] Y. K. Park, S. B. Choi, H. Kim, K. Kim, B. H. Won, K. Choi, J. S. Choi, W. S. Ahn, N. Won, S. Kim, D. H. Jung, S. H. Choi, G. H. Kim, S. S. Cha, Y. H. Jhon, J. K. Yang, J. Kim, *Angew. Chem., Int. Ed.* **2007**, *46*, 8230.
[11] D. Feng, T. F. Liu, J. Su, M. Bosch, Z. Wei, W. Wan, D. Yuan, Y. P. Chen, X. Wang, K. Wang, X. Lian, Z. Y. Gu, J. Park, X. Zou, H. C. Zhou, *Nat. Commun.* **2015**, *6*, 5979.
[12] Y. Lv, W. Zhan, Y. He, Y. Wang, X. Kong, Q. Kuang, Z. Xie, L. Zheng, *ACS Appl. Mater. Interfaces* **2014**, *6*, 4186.
[13] D. Bradshaw, S. El-Hankari, L. Lupica-Spagnolo, *Chem. Soc. Rev.* **2014**, *43*, 5431.
[14] Y. Zhao, J. Zhang, B. Han, J. Song, J. Li, Q. Wang, *Angew. Chem., Int. Ed.* **2011**, *50*, 636.
[15] L. B. Sun, J. R. Li, J. Park, H. C. Zhou, *J. Am. Chem. Soc.* **2012**, *134*, 126.
[16] H. Huang, J. R. Li, K. Wang, T. Han, M. Tong, L. Li, Y. Xie, Q. Yang, D. Liu, C. Zhong, *Nat. Commun.* **2015**, *6*, 8847.
[17] L. Feng, J. L. Li, G. S. Day, X. L. Lv, H. C. Zhou, *Chem* **2019**, *5*, 1265.
[18] G. G. Chang, X. C. Ma, Y. X. Zhang, L. Y. Wang, G. Tian, J. W. Liu, J. Wu, Z. Y. Hu, X.-Y. Yang, B. Chen, *Adv. Mater.* **2019**, *31*, 1904969.
[19] L. Feng, S. Yuan, L.-L. Zhang, K. Tan, J.-L. Li, A. Kirchon, L.-M. Liu, P. Zhang, Y. Han, Y. J. Chabal, H.-C. Zhou, *J. Am. Chem. Soc.* **2018**, *140*, 2363.
[20] G. Cai, H.-L. Jiang, *Angew. Chem., Int. Ed.* **2017**, *56*, 563.
[21] V. Guillerm, H. Xu, J. Albalad, I. Imaz, D. Maspoch, *J. Am. Chem. Soc.* **2018**, *140*, 15022.
[22] C. Avci, J. Arinez-Soriano, A. Carne-Sanchez, V. Guillerm, C. Carbonell, I. Imaz, D. Maspoch, *Angew. Chem., Int. Ed.* **2015**, *54*, 14417.
[23] S. Yuan, L. Zou, J.-S. Qin, J. Li, L. Huang, L. Feng, X. Wang, M. Bosch, A. Alsalme, T. Cagin, H.-C. Zhou, *Nat. Commun.* **2017**, *8*, 15356.
[24] L. Peng, J. Zhang, Z. Xue, B. Han, X. Sang, C. Liu, G. Yang, *Nat. Commun.* **2014**, *5*, 4456.
[25] X.-Y. Yang, L.-H. Chen, Y. Li, J. C. Rooke, C. Sanchez, B.-L. Su, *Chem. Soc. Rev.* **2017**, *46*, 481.
[26] J. Koo, I.-C. Hwang, X. Yu, S. Saha, Y. Kim, K. Kim, *Chem. Sci.* **2017**, *8*, 6799.
[27] W. Zhang, Y. Liu, G. Lu, Y. Wang, S. Li, C. Cui, J. Wu, Z. Xu, D. Tian, W. Huang, J. S. DuCheneu, W. D. Wei, H. Chen, Y. Yang, F. Huo, *Adv. Mater.* **2015**, *27*, 2923.
[28] Y. Y. Xiao, X. L. Liu, G. G. Chang, C. Pu, G. Tian, L. Y. Wang, J. W. Liu, X. C. Ma, X.-Y. Yang, B. Chen, *Nanoscale* **2020**, *12*, 6250.
[29] L. Feng, K.-Y. Wang, J. Powell, H.-C. Zhou, *Matter* **2019**, *1*, 801.
[30] S. Feng, W. Li, Q. Shi, Y. Li, J. Chen, Y. Ling, A. M. Asiri, D. Zhao, *Chem. Commun.* **2014**, *50*, 329.
[31] Y. Kim, T. Yang, G. Yun, M. B. Ghasemian, J. Koo, E. Lee, S. J. Cho, K. Kim, *Angew. Chem., Int. Ed.* **2015**, *54*, 13273.
[32] D. Zhao, D. J. Timmons, D. Yuan, H.-C. Zhou, *Acc. Chem. Res.* **2011**, *44*, 123.
[33] T. Zhao, S. H. Li, Y. X. Xiao, C. Janiak, G. G. Chang, G. Tian, X.-Y. Yang, *Sci. China Mater.* **2020**, *64*, 252.
[34] M. Taddei, K. C. Dümbgen, J. A. van Bokhoven, M. Ranocchiari, *Chem. Commun.* **2016**, *52*, 6411.
[35] T. He, X. Xu, B. Ni, H. Wang, Y. Long, W. Hu, X. Wang, *Nanoscale* **2017**, *9*, 19209.

[36] F. Ragon, P. Horcajada, H. Chevreau, Y. K. Hwang, U.-H. Lee, S. R. Miller, T. Devic, J.-S. Chang, C. Serre, *Inorg. Chem.* **2014**, *53*, 2491.
[37] A. Schaate, P. Roy, A. Godt, J. Lippke, F. Waltz, M. Wiebcke, P. Behrens, *Chem. - Eur. J.* **2011**, *17*, 6643.
[38] M. J. Cliffe, W. Wan, X. Zou, P. A. Chater, A. K. Kleppe, M. G. Tucker, H. Wilhelm, N. P. Funnell, F.-X. Coudert, A. L. Goodwin, *Nat. Commun.* **2014**, *5*, 4176.
[39] P. Niu, N. Lua, J. Liu, H. Jia, F. Zhou, B. Fan, R. Li, *Microporous Mesoporous Mater.* **2019**, *281*, 92.
[40] J. H. Cavka, S. Jakobsen, U. Olsbye, N. Guillou, C. Lamberti, S. Bordiga, K. P. Lillerud, *J. Am. Chem. Soc.* **2008**, *130*, 13850.
[41] H. Wu, Y. S. Chua, V. Krungleviciute, M. Tyagi, P. Chen, T. Yildirim, W. Zhou, *J. Am. Chem. Soc.* **2013**, *135*, 10525.
[42] F. Vermoortele, B. Bueken, G. L. Bars, B. Van de Voorde, M. Vandichel, K. Houthoofd, A. Vimont, M. Daturi, M. Waroquier, V. Van Speybroeck, C. Kirschhock, D. E. De Vos, *J. Am. Chem. Soc.* **2013**, *135*, 11465.
[43] S. Cherian, C. C. Wamser, *J. Phys. Chem. B* **2000**, *104*, 3624.
[44] M. A. Bos, Z. Shervani, A. C. I. Anusiem, M. Giesbers, W. Norde, J. M. Kleijn, *Colloids Surf., B* **1994**, *3*, 91.
[45] H. An, M. Li, J. Gao, Z. Zhang, S. Ma, Y. Chen, *Coord. Chem. Rev.* **2019**, *384*, 90.